Numerical and Experimental Validation of the Passive Performance of a Coharmonic Gyro-Multiplier Interaction Region

David A. Constable, Alan D. R. Phelps, *Member, IEEE*, Colin G. Whyte, Wenlong He, Adrian W. Cross, *Member, IEEE*, and Kevin Ronald, *Member, IEEE*

***Abstract*— The azimuthally rippled cavity for a large-orbit, coharmonic gyro-multiplier, designed to operate at the second and fourth harmonics, at frequencies of 37.5 and 75 GHz, respectively, has been numerically and experimentally confirmed to be insensitive to the polarization of quadrupole, $TE_{2,n}$-like modes, including the second-harmonic operating mode of the multiplier, a cylindrical $TE_{2,2}$-like waveguide mode. To test the cavity with this mode required the design, construction, and measurement of ripple wall mode converters, converting the cylindrical $TE_{2,1}$ mode into the $TE_{2,2}$ mode. These were designed to operate at a central frequency of ∼37.9 GHz, with predicted mode purity of better than 85%, and 3-dB bandwidth of 161 MHz. The constructed converter had a central operating frequency of 37.7 GHz, with *S*-parameter measurements used to infer suitable mode purity and an operational 3-dB bandwidth of 50 MHz. This has allowed far-field phase measurements of the corrugated cavity to be conducted, where the orientation of the geometry to the polarization of both the $TE_{2,1}$ and $TE_{2,2}$ modes was shown to have no effect on the dispersion.**

***Index Terms*— Cyclotron resonant masers, electromagnetism, gyrotrons, microwave measurements, mode convertors.**

I. Introduction

GYRO-MULTIPLIERS [1]–[5] represent an attractive method of obtaining coherent high-frequency radiation, which can extend into the THz regime [6], [7]. Reliable microwave sources operating in this regime will facilitate the growing number of applications emerging across a range of diverse fields, such as communications [8], [9], spectroscopy [10], and medicine [6], [11]–[14].

Gyro-multipliers are an extension of the gyrotron [15]–[17], where an electron beam immersed in an axial magnetic field will emit coherent radiation close to the electron cyclotron frequency, ω_{ce} (1), as dictated by the dispersion relation (2). Here, e is the electron charge, B_z is the strength of the axial magnetic field, γ is the relativistic correction factor, m_0 is the rest mass of the electron, s ($\in \mathbb{Z}$) is the cyclotron harmonic, k_z is the axial wavenumber, and υ_z is the axial velocity of the electron beam

$$\omega_{\mathrm{ce}} = \frac{eB_z}{\gamma m_0} \tag{1}$$

$$\omega = s\omega_{\mathrm{ce}} + k_z\upsilon_z \tag{2}$$

Two distinct types of gyro-multiplier exist: single-cavity [18]–[21] and multiple-cavity [22]–[28] arrangements, with both oscillator and amplifier configurations being investigated. Both systems operate in a similar manner, by tuning the geometry of the device correctly, directly exciting a low-harmonic signal resulting in modulation of the azimuthal current on the beam at the "driven" harmonic and at multiples of that harmonic. The harmonic output is not directly excited (which is difficult to achieve for harmonics >3) but is instead parasitically emitted. Considering (1) and (2), using high-harmonic operation ($s > 1$) results in a reduced magnetic field compared with low-harmonic operation at the same frequency. Therefore, the ancillary system requirements of the gyro-multiplier can be reduced. This is of particular importance at high frequencies, where the limits of magnet technology become challenging. This process is known as coharmonic behavior [18]–[20]. In a large-orbit gyrotron (LOG), the azimuthal mode index, m, corresponding to the number of full-wave variations in the radial component of the field amplitude in a closed azimuthal path around the waveguide axis must equal the harmonic number, s. There is no natural harmonic relationship in the mode spectrum of cylindrical waveguides, that is, two modes, with an integer ratio of their azimuthal indices, will not have an integer ratio of their cutoff frequencies. A special arrangement for the cavity is therefore required to enable simultaneous direct excitation at the low harmonic and emission at the high harmonic.

Manuscript received January 13, 2021; revised April 7, 2021 and May 19, 2021; accepted June 12, 2021. Date of publication July 16, 2021; date of current version October 5, 2021. This work was supported by the Engineering and Physical Sciences Research Council (EPSRC) under Grant EP/R004773/1 and Grant EP/R034737/1. The work of David A. Constable was supported by a Ph.D. studentship from the U.K. Engineering and Physical Sciences Research Council (EPSRC). *(Corresponding author: David A. Constable.)*

David A. Constable was with SUPA, Department of Physics, University of Strathclyde, Glasgow G4 0NG, U.K. He is now with the Physics Department, Lancaster University, Lancaster LA1 4YW, U.K. (e-mail: d.constable@lancaster.ac.uk).

Alan D. R. Phelps, Colin G. Whyte, Adrian W. Cross, and Kevin Ronald are with SUPA, Department of Physics, University of Strathclyde, Glasgow G4 0NG, U.K. (e-mail: a.d.r.phelps@strath.ac.uk; colin.whyte@strath.ac.uk; a.w.cross@strath.ac.uk; k.ronald@strath.ac.uk).

Wenlong He was with SUPA, Department of Physics, University of Strathclyde, Glasgow, G4 0NG, U.K. He is now with the College of Electronic and Information Engineering, Shenzhen University, Shenzhen 518060, Guangdong Province, China (e-mail: wenlong.he@szu.edu.cn).

Color versions of one or more figures in this article are available at https://doi.org/10.1109/TMTT.2021.3094219.

Digital Object Identifier 10.1109/TMTT.2021.3094219

0018-9480 © 2021 IEEE. Personal use is permitted, but republication/redistribution requires IEEE permission.
See https://www.ieee.org/publications/rights/index.html for more information.

Authorized licensed use limited to: University of York. Downloaded on August 29,2024 at 10:33:34 UTC from IEEE Xplore. Restrictions apply.

In this article, we discuss the passive performance of an azimuthally corrugated interaction region for use in a large-orbit gyro-multiplier. Azimuthal corrugations in gyrotron interaction regions have also been examined in small-orbit devices (e.g., [29]), to break the degeneracy of nonsymmetric modes. In these cases, there have been impacts noted on the interaction efficiency. In the present case, the intention is that the corrugation should not affect the degeneracy of the two polarizations associated with the lower harmonic resonance, hence not affecting the beneficial coupling to the large-orbit electron beam.

The performance of a large-orbit, corrugated cavity gyro-multiplier oscillator, operating at the second and fourth harmonics, has previously been numerically simulated with the particle-in-cell code, MAGIC3-D [20], [30], as well as measured experimentally, with an electron beam [19]. Both PIC simulations and experiment demonstrated successful coharmonic operation, with signals excited at 37.5 and 75 GHz, in the $TE_{2,2}$-like and $TE_{4,3}$-like waveguide modes, respectively. A short cutoff taper leading to a section of circular waveguide was intended to trap the second-harmonic $TE_{2,2}$-like signal within the cavity, thus allowing output of a pure $TE_{4,3}$ mode. However, it was observed that the $TE_{2,2}$ mode underwent mode conversion along the output taper, converting into the $TE_{2,1}$ and $TM_{2,1}$ waveguide modes, which were above cutoff in the output region. In previous discussions of the coharmonic interaction region, its passive performance has not been validated; specifically, the insensitivity of the orientation of the corrugation to the $TE/TM_{2,n}$ modes has not been documented, either numerically or experimentally.

In this article, we present numerical simulations and experimental measurement demonstrating the insensitivity of the mode cutoff frequency to the corrugation's alignment to the polarization of the $TE_{2,2}$ mode. To achieve this, the authors use a previously documented $TE_{2,1}$ mode launcher [31] in combination with a ripple wall mode converter [32]–[34], to generate a $TE_{2,2}$ waveguide mode. This waveguide mode is then used to examine the response of the cavity to the two lowest quadrupole $TE_{2,n}$ modes. Numerical simulations from CST Microwave Studio are also carried out to show the sensitivity of the octopole ($TE_{4,n}$) modes to the orientation of the cavity corrugation.

II. Basic Principles

The corrugated region of the gyro-multiplier features an eightfold sinusoidal corrugation, as shown in Fig. 1, which is intended to break the degeneracy of the two polarizations of the $TE_{4,3}$ waveguide mode (used for the high-frequency output at the fourth harmonic), that is, separating their cutoff frequencies. In this article, polarization refers to the two orthogonal polarizations that one would expect to occur in a standard cylindrical waveguide. The corrugation can be refined to allow the higher of the two $TE_{4,3}$-like modes to be cutoff at exactly double the frequency of the $TE_{2,2}$-like mode, which is intended to be excited at the second harmonic by a cyclotron electron beam. However, the degeneracy of the polarizations of the $TE_{2,2}$-like mode should not be affected by corrugation.

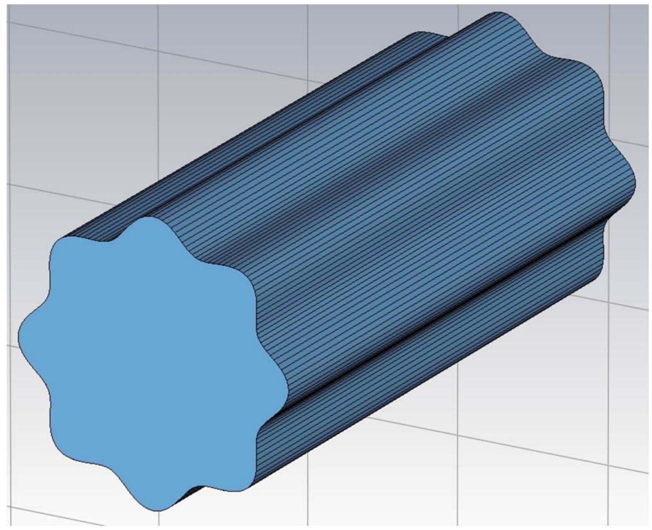

Fig. 1. Representation of the coharmonic corrugated waveguide, from CST Microwave Studio.

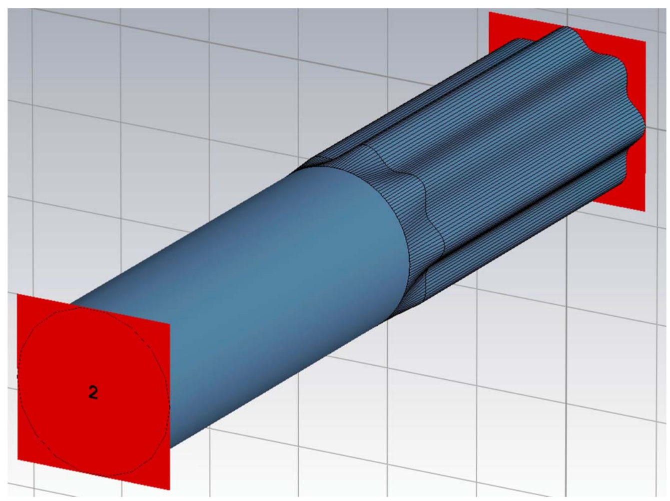

Fig. 2. Geometry simulated in CST Microwave Studio.

The cavity has an average radius of 8 mm, with a corrugation depth of 0.7 mm. The corrugation profile follows (3), where ϕ is the azimuthal coordinate, varying between 0 and 2π. The output region is cylindrical, with a radius of 8.3 mm. The cutoff frequency for a cylindrical waveguide can be determined from (4), where c is the speed of light in vacuum; $p'_{m,n}$ is the "nth" root of the differentiated Bessel function of the first kind, of order "m" (6.706 for the $TE_{2,2}$ mode and 12.682 for the $TE_{4,3}$ mode); and r is the radius of the waveguide under consideration. In the output region, the cutoff frequency of the $TE_{2,2}$ mode is 38.4 GHz, while it is 72.9 GHz for the $TE_{4,3}$ mode

$$r(\phi) = (8 + 0.7\sin(8\phi))[\mathrm{mm}] \tag{3}$$

$$f_{\mathrm{cutoff}} = \frac{cp'_{m,n}}{2\pi r} \tag{4}$$

The effect of corrugation on the $TE_{2,2}$-like and $TE_{4,3}$-like modes is initially investigated in CST Microwave Studio. The simulated geometry is shown in Fig. 2. Here, the cavity is

Authorized licensed use limited to: University of York. Downloaded on August 29,2024 at 10:33:34 UTC from IEEE Xplore. Restrictions apply.

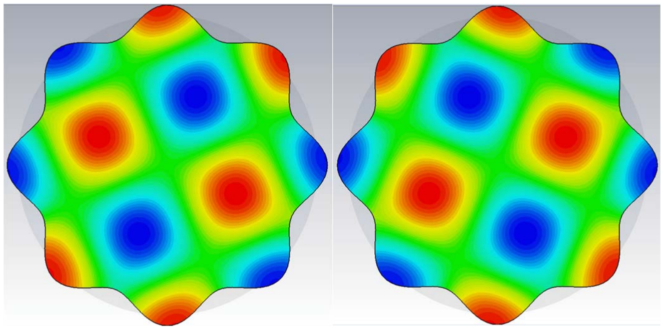

Fig. 3. Magnitude of the axial magnetic field for the two polarizations of the $TE_{2,2}$-like mode in the corrugated waveguide, from CST Microwave Studio.

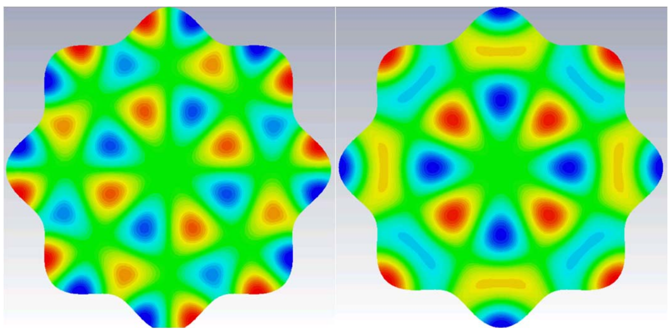

Fig. 4. Magnitude of the axial magnetic field for the two polarizations of the $TE_{4,3}$-like mode in the corrugated waveguide, from CST Microwave Studio.

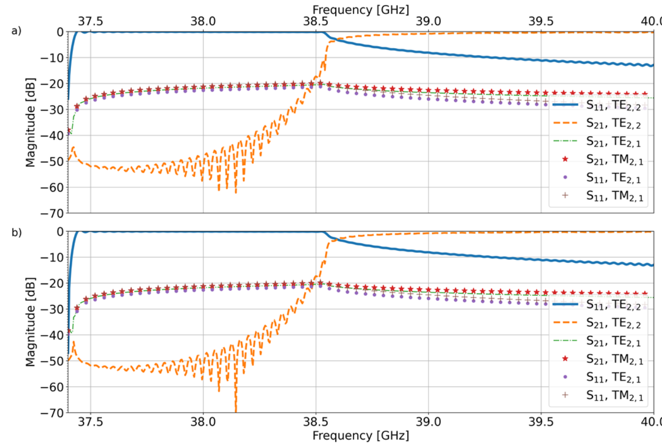

Fig. 5. Predictions of the S-parameters for launching of (a) first and (b) second polarizations of the $TE_{2,2}$ mode, into the simulated geometry, from CST Microwave Studio.

39 mm in length, the output taper is 6 mm in length, and the cylindrical waveguide is 45 mm in length. The taper is a linear transition between the radii of the corrugation and the smooth bore cylindrical waveguide (radius 8.3 mm). The required modes are excited at port 1, which terminates the corrugated region. The mesh used in all CST Microwave Studio discussed in this article is hexahedral, comprising ~4050 cells per mm^3. No Ohmic losses are considered in any CST Microwave Studio simulation presented in this article.

An important feature of the corrugation is that the two polarizations of quadrupole ($TE_{2,n}$) modes perceive the same effective radius, r_{eff}, and thus remain degenerate. CST Microwave Studios' evaluation of the cutoff condition for the two polarizations (with a frequency of 37.426 GHz, corresponding to $r_{\text{eff}} = 8.55$ mm) verifies this insensitivity to the eightfold corrugation. The amplitude of the axial magnetic field component for the two polarizations of the $TE_{2,2}$-like modes within the corrugated region is shown in Fig. 3. Here, the two mode patterns are identical to each other, apart from a simple azimuthal rotation of $\pi/8$, as expected for a quadrupole mode.

In contrast, the degeneracy of the two polarizations of the octopole ($TE_{4,n}$) mode will be broken by the corrugation. Fig. 4 shows the variation in the amplitude of the axial components of the magnetic field for the two polarizations of the $TE_{4,3}$-like mode within the corrugated waveguide. As can be seen, there is a definite difference between the two magnetic field distributions, with a splitting of the degeneracy of the cutoff frequencies of the two polarizations. Here, one cannot simply transform between the two polarizations by azimuthal rotation. CST Microwave Studio predicts the cutoff frequencies of the two polarizations to be 69.5 and 75.2 GHz, respectively. Using (4), the effective radii for the two polarizations of the $TE_{4,3}$-like waveguide modes within the corrugated waveguide are 8.70 and 8.05 mm, respectively.

The insensitivity of the $TE_{2,2}$-like modes and the sensitivity of the $TE_{4,3}$-like modes can further be demonstrated through the S-parameters predicted by time-domain simulations. Here, the two distinct polarizations of the $TE_{2,2}$-like and $TE_{4,3}$-like modes are injected at port 1 in the geometry shown in Fig. 2, with the reflection (S_{11}) and transmission (S_{21}) parameters predicted.

Fig. 5 shows the near-identical predictions of the S-parameters for both polarizations of the $TE_{2,2}$ mode (previously seen in Fig. 3), across a frequency range of 37.4–40 GHz. The polarization of the $TE_{2,1}$ and $TM_{2,1}$ modes is dictated by the polarization of the injected $TE_{2,2}$ mode. All other modes are observed at levels of less than −40 dB and are thus ignored.

Between 37.4 and 38.5 GHz, the incident mode shows a strong reflection (S_{11}, $TE_{2,2}$) close to 0 dB, as it is reflected due to the cutoff taper at the output end of the waveguide. However, mode conversion occurs along the length of the cutoff taper, resulting in the $TE_{2,1}$ and $TM_{2,1}$ modes being reflected to the input port (S_{11}, $TE_{2,1}$ and S_{11}, $TM_{2,1}$) and transmitted to the output port (S_{21}, $TE_{2,1}$ and S_{21}, $TM_{2,1}$). The degree of mode conversion is on the order of −20 to −40 dB for all frequencies above 37.4 GHz and is consistent with the MAGIC3-D simulations reported in [20]. Below the cutoff frequency of the $TE_{2,2}$ mode, the reflection and transmission predicted for each mode converted signal are approximately equal (e.g., at 37.6 GHz, the magnitude of S_{21} of $TE_{2,1} \sim S_{11}$ of $TE_{2,1}$). The alternative orthogonal polarization of the quadrupole mode is not observed at any significant level, due to the linear polarization of the injected signal.

Fig. 6 shows the S-parameter predictions for the launching of two polarizations of the $TE_{4,3}$ mode, across a frequency range of 70–80 GHz and 75–80 GHz, respectively. On comparing the two plots, it is evident that the two polarizations have distinct S-parameters. The first polarization [Fig. 6(a)] is

Authorized licensed use limited to: University of York. Downloaded on August 29,2024 at 10:33:34 UTC from IEEE Xplore. Restrictions apply.

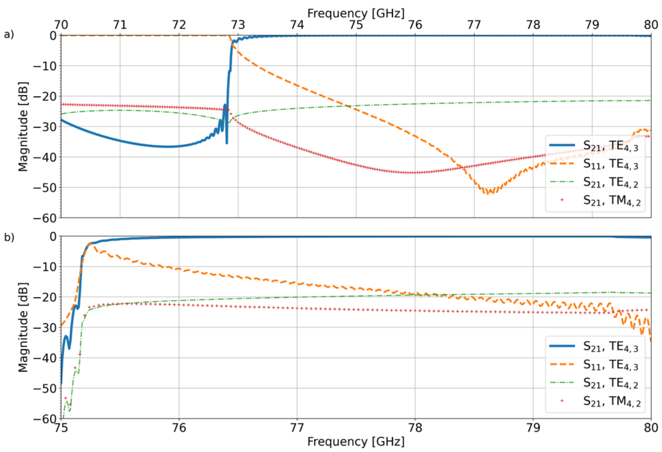

Fig. 6. Predictions of the S-parameters for launching of (a) first and (b) second polarizations of the $\mathrm{TE}_{4,3}$ mode, into the simulated geometry, from CST Microwave Studio.

strongly reflected for frequencies less than 72.9 GHz, as it is cutoff in the cylindrical output region. In this polarization, $\mathrm{TE}_{4,3}$ has a cutoff frequency in the corrugated waveguide of 69.7 GHz, allowing it to propagate. Above 72.9 GHz, the $\mathrm{TE}_{4,3}$ mode propagates unimpeded to the output. It is important to note that mode conversion along the output taper occurs for the $\mathrm{TE}_{4,2}$ mode across the entire frequency range, at levels less than -20 dB. Mode conversion is observed to lower order $\mathrm{TE}_{4,n}$ and $\mathrm{TM}_{4,n}$ modes, but at levels of less than -40 dB and are thus not considered.

In comparison, the second polarization of the $\mathrm{TE}_{4,3}$ mode is cutoff within the corrugated waveguide [Fig. 6(b)], below a frequency of 75.1 GHz, with no signals propagating below this. This is in good agreement with the expected cutoff frequency of a cylindrical waveguide of radius $\sim$8.07 mm. For frequencies above 75.1 GHz, this polarization is largely transmitted to the output, with some of the signal reflected to the input (S_{11}, $\mathrm{TE}_{4,3}$), the magnitude of which decreases with increasing frequency. Mode conversion again occurs along the output taper, with the $\mathrm{TE}_{4,2}$ and $\mathrm{TM}_{4,2}$ modes being the dominant of the converted signals. Again, all other modes are predicted to have signals of less than -40 dB and are ignored.

III. Ripple Wall Mode Converter

To generate the circular waveguide $\mathrm{TE}_{2,2}$ mode necessary to experimentally cold-test the corrugated waveguide (Fig. 1) discussed in Section II, a set of mode converting structures were required. Ripple wall mode converters feature an axial perturbation [32]–[34] and have previously been used to change the radial mode index of an electromagnetic signal in an over-moded cylindrical waveguide. The axial perturbation varies sinusoidally in radius, with the perturbation period, L, being close to the beat wavelength, λ_{beat}, of the incident and desired modes in unperturbed waveguide, as shown in (5), where β_1 and β_2 are the wavenumbers of the incident ($\mathrm{TE}_{2,1}$) and converted ($\mathrm{TE}_{2,2}$) signals, respectively [35], [36]. The conversion efficiencies of ripple wall mode converters are often close to 100%, with their bandwidth being determined

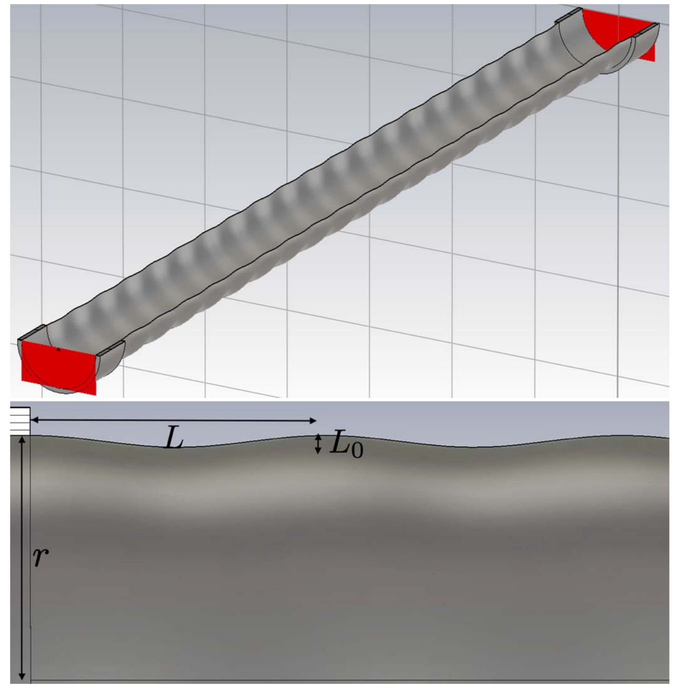

Fig. 7. Cross-sectional view of the $\mathrm{TE}_{2,1}$ to $\mathrm{TE}_{2,2}$ mode converter, as represented by CST Microwave Studio.

by the number of periods used [36]–[38]. The maximum bandwidth can be obtained through a single period equal to a beat wavelength [37]; however, the need for bandwidth must be balanced against the need to suppress any unwanted modes [36]

$$\lambda_{\text{beat}} = \frac{2\pi}{\beta_1 - \beta_2} \tag{5}$$

As described previously, the second harmonic of the coharmonic gyrotron is intended to operate at a frequency of $\sim$37.5 GHz, in the $\mathrm{TE}_{2,2}$ mode. Since the cutoff frequency of the $\mathrm{TE}_{2,2}$ mode in the output region of the corrugated waveguide is $\sim$38.4 GHz, the ripple wall mode converter was optimized to operate between these frequencies so that it can be used to test the predicted leakage of signal through the mode conversion process.

A. Design and Numerical Simulation

CST Microwave Studio was used to optimize the design of the ripple wall mode converter. The input and output radii were both chosen to be 8.7 mm, with a sinusoidal ripple in the radius of the tube between the two ports. The parameters in the optimization process were the depth and period of the ripple, and the number of periods. The optimization goal was set for maximum excitation of the $\mathrm{TE}_{2,2}$ signal at the output port, induced by the $\mathrm{TE}_{2,1}$ mode at the input port. As in Section II, no Ohmic losses are considered.

The optimized mode converter is shown in Fig. 7. Here, the smooth bore sections at either end are visible, with the vertical planes depicting the incoming and outgoing ports in CST Microwave Studio. Since the device is symmetrical, the ports can be considered interchangeable. The optimized

Authorized licensed use limited to: University of York. Downloaded on August 29,2024 at 10:33:34 UTC from IEEE Xplore. Restrictions apply.

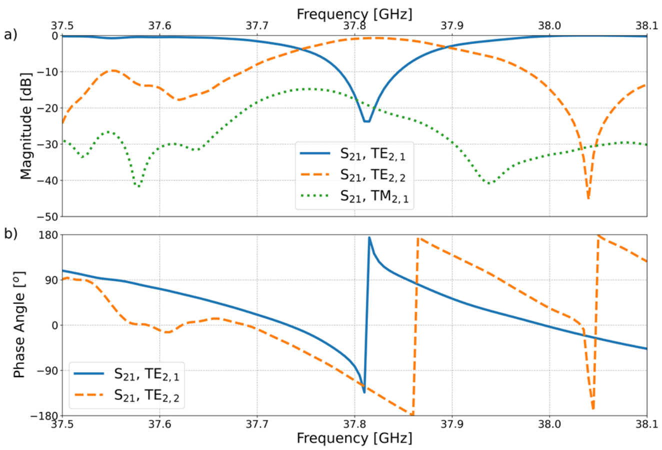

Fig. 8. S_{21} parameters of the $TE_{2,1}$-to-$TE_{2,2}$ mode converter, as predicted by CST Microwave Studio. (a) shows the forward transmission signal, and (b) shows the phase angle evolution.

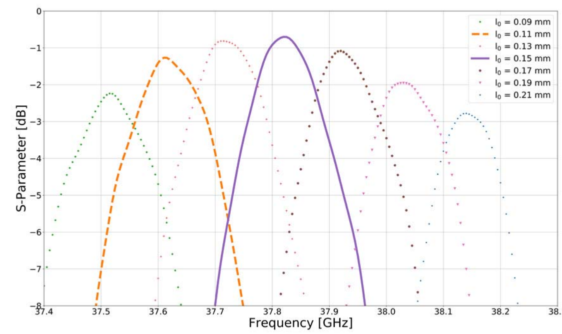

Fig. 9. Variation in the S_{21} parameters of the $TE_{2,2}$ mode produced by the $TE_{2,1}$-to-$TE_{2,2}$ mode converter, as a function of ripple amplitude, as predicted by CST Microwave Studio.

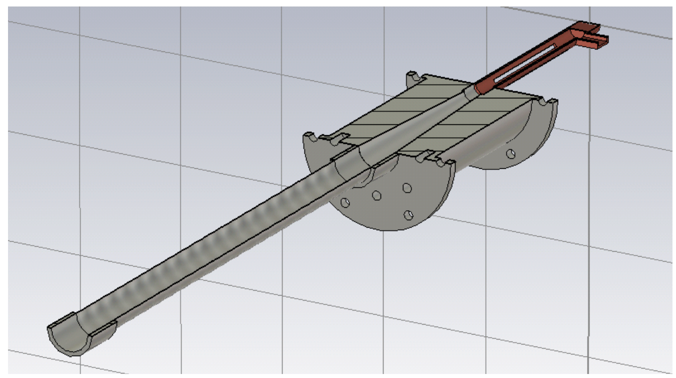

Fig. 10. Cross-sectional view of the setup for measuring the $TE_{2,1}$-to-$TE_{2,2}$ mode converters (note, the second $TE_{1,0}$-to-$TE_{2,1}$ mode converter and taper are not shown).

parameters are a ripple depth of $L_0 = 0.15$ mm, 20 periods, and a period of $L = 10.5$ mm. The period, L, is close to the beat wavelength of the two signals, $\lambda_{\text{beat}} = 9.2$ mm. It has previously been documented that if unwanted modes are present, a larger number of periods are required to obtain the desired mode purity of the chosen mode [36]. This has informed the choice of a large number of periods in this design, due to the need to suppress conversion to the undesired $TM_{2,1}$ mode, and subsequently resulting in a narrow bandwidth device. A pure $TE_{2,1}$ signal, across a frequency span of 35–40 GHz, is provided as the input signal, with the S-parameters at both ports recorded.

The predicted S_{21} parameters for the mode converter are shown in Fig. 8(a). A constrained range of frequencies between 37.5 and 38.5 GHz is considered. Here, the solid curve shows the injected $TE_{2,1}$ mode and the dashed curve shows the $TE_{2,2}$ mode. As can be seen, a strong conversion to the desired mode is predicted at a level better than -0.7 dB (~85.1% power conversion), at a center frequency of ~37.82 GHz. The 3-dB bandwidth of the converted signal is 161 MHz. Weak conversion is also observed to the undesired $TM_{2,1}$ mode (dotted curve); however, this is predicted at a relative magnitude of less than -15 dB across the entire frequency range.

The phase evolution of the $TE_{2,1}$ and $TE_{2,2}$ modes predicted at the output of the converter is depicted in Fig. 8(b). For much of the frequency span, the phase of the $TE_{2,1}$ signal evolves smoothly. However, around 37.8 GHz, there is a sudden change in the gradient of the phase angle in the range where energy is being scattered to the $TE_{2,2}$ mode. Conversely, the $TE_{2,2}$ signal exhibits numerous complex fluctuations in its relative phase at frequencies corresponding to the peaks and troughs in its transmission behavior, exhibiting regular dispersive behavior in the region from 37.7 to 38.0 GHz, where the signal is strong.

Small variations in the period of the structure show little impact on the operation of the mode converter; however, slight variations in the amplitude of the ripple are predicted to have a significant effect. Fig. 9 depicts the transmission of the $TE_{2,2}$ signal, as a function of the ripple amplitude for variations spanning ± 60 μm in steps of 20 μm, around the optimized value of 150 μm. As can be seen, these small variations in the amplitude result in changes in both the central frequency of operation and a reduction in the magnitude of the converted signal.

B. Experimental Testing

Following their design, two aluminum formers for the mode converter structure were formed using a computer numerical controlled (CNC) lathe, which had a machining tolerance of ± 10 μm. A 5-mm layer of copper was grown on top of the aluminum, with the aluminum then etched out, leaving the shape of the mode converter. To confirm the performance of the mode converter, its S-parameter behavior was measured using an Anritsu VectorStar MS4644A Vector Network Analyzer (VNA), across a frequency range of 37.5–40 GHz. The experimental setup used is similar to that shown in Fig. 10, where a $TE_{2,1}$ mode launcher [30] is shown feeding into a linear taper (tapering from a radius of 3.96 to 8.7 mm over a length of 50 mm) and connected to the ripple wall mode converter. The choice of linear taper geometry was to maintain mode purity of the $TE_{2,1}$ signal, having been confirmed by simulations in CST Microwave Studio. To perform transmission measurements, an identical taper and launcher are positioned on the opposing side of the ripple

Authorized licensed use limited to: University of York. Downloaded on August 29,2024 at 10:33:34 UTC from IEEE Xplore. Restrictions apply.

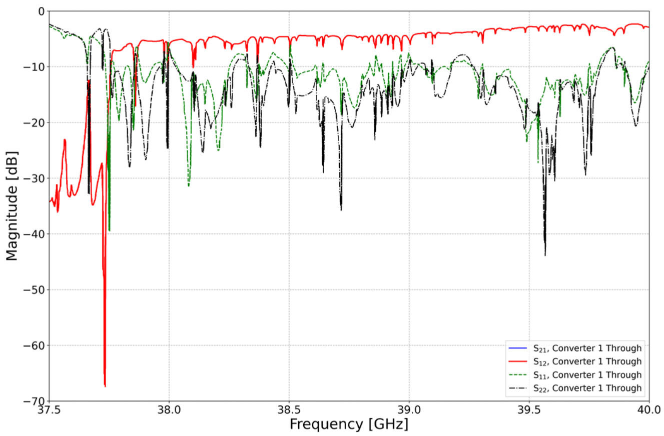

Fig. 11. Measured S-parameters of the $TE_{2,1}$-to-$TE_{2,2}$ mode converters. S_{21} and S_{12} curves are overlayed.

wall mode converter. The network analyzer was calibrated with its reference planes at the WR28 rectangular waveguide ports which connect to the input ports of the $TE_{2,1}$ launchers. As a result, the measurements incorporate the loss resulting from the $TE_{2,1}$ launchers.

The $TE_{2,2}$ mode has a cutoff frequency of 79.9 GHz within the $TE_{2,1}$ waveguide launcher, and therefore cannot propagate within that structure. To examine the transmission performance of the ripple wall mode converter, sudden increases in the magnitude of the reflection parameters are identified. Such increases correspond to frequencies at which the converted $TE_{2,2}$ signal is reflected from the cutoff aperture at the far end of the ripple wall convertor, and then reconverted to a $TE_{2,1}$ signal in its reverse transit. This signal will travel back to the incoming port and will therefore present itself as an increase in the reflected signal at that frequency and would be expected to correspond to a minimum in the transmission.

The measured transmission and reflection performances of one of the ripple wall mode converters are shown in Fig. 11. Here, the solid curve depicts the forward (S_{21}) and reverse (S_{12}) transmission behavior, while the dashed and dot-dash curves show the forward (S_{11}) and reverse (S_{22}) reflection performance, respectively. The transmission measurements demonstrate reciprocity.

Around 37.7–37.8 GHz, the transmitted signal shows a significant decrease in magnitude of −20 dB, associated with a high reflection signal, as one would expect for the intended mode conversion process. At higher frequencies, there are small drops in the transmitted signal of −3 dB, indicating weak mode conversion to some higher order mode. The $TE_{2,1}$ mode was previously measured in isolation and showed good transmission (5-dB loss, due to signal being radiated through azimuthal slots designed to force coupling to the required mode) down to a frequency of 37.6 GHz [31]. Hence, the sharp drop in the transmission signal shown in Fig. 11 at 37.7 GHz must be associated with the excitation of the $TE_{2,2}$ mode in the convertor. The bottom end of the conversion band nearly overlapped with the minimum frequency supported by the $TE_{2,1}$ launchers, so one only sees a partial (and sharp) recovery in the transmission behavior as the frequency drops to 37.6 GHz.

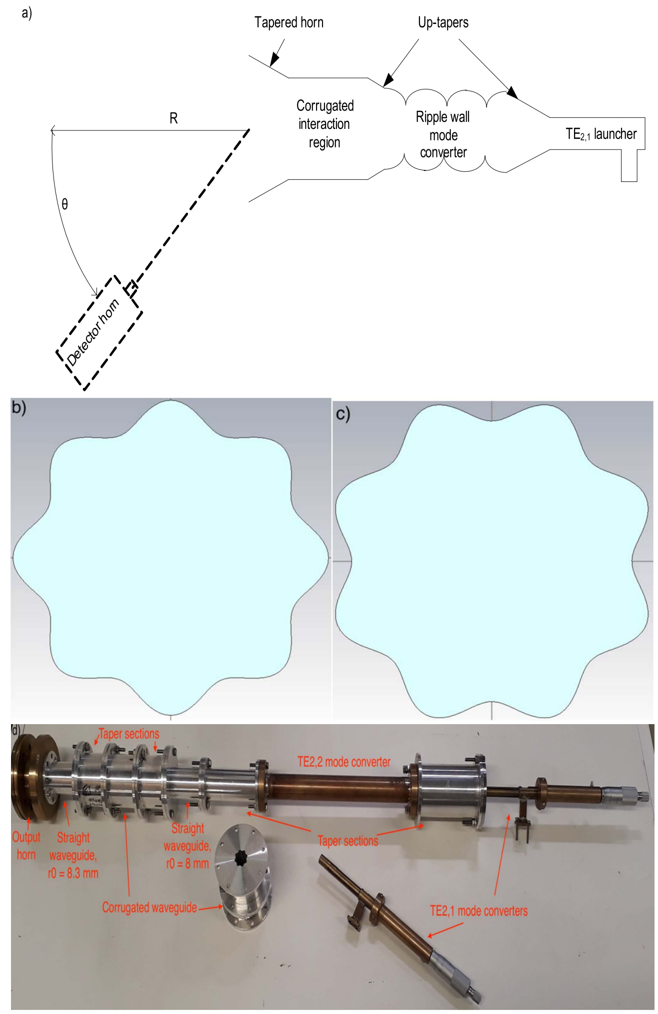

Fig. 12. Representations of (a) schematic of the experimental setup and the corrugated waveguide orientated at (b) $\varphi = 0°$, (c) $\varphi = 22.5°$, and (d) launching apparatus. Also visible in (d) is the corrugated waveguide.

IV. Millimeter Wave Measurements of the Azimuthally Corrugated Waveguide

Following the successful demonstration of the generation of $TE_{2,1}$ and $TE_{2,2}$ modes, millimeter-wave measurements of the coharmonic corrugated waveguide could be conducted. This process was performed by fixing the position of a receiving antenna in the far-field and recording phase information from the open end of the cavity, which itself was tapered (up in radius) to an above cutoff section of waveguide for the purpose of this test. To ensure the converted $TE_{2,2}$ signal is not close to the cutoff at the output aperture, a horn antenna was designed for the mode converter. The linearly tapered antenna has an input radius of 8.7 mm, an output radius of 26.4 mm, and a length of 50 mm. The experimental setup for this is shown in Fig. 12(a), with the launching apparatus shown in Fig. 12(d). Since the corrugation has an azimuthal period of 45°, measurements are conducted with the cavity aligned at orientations of 0° and 22.5°, with respect to the polarization of the $TE_{2,1}$ launcher. The two orientations of the cavity are shown in Fig. 12(b) and (c), respectively. This measurement is conducted both with the ripple wall mode converter and

Authorized licensed use limited to: University of York. Downloaded on August 29,2024 at 10:33:34 UTC from IEEE Xplore. Restrictions apply.

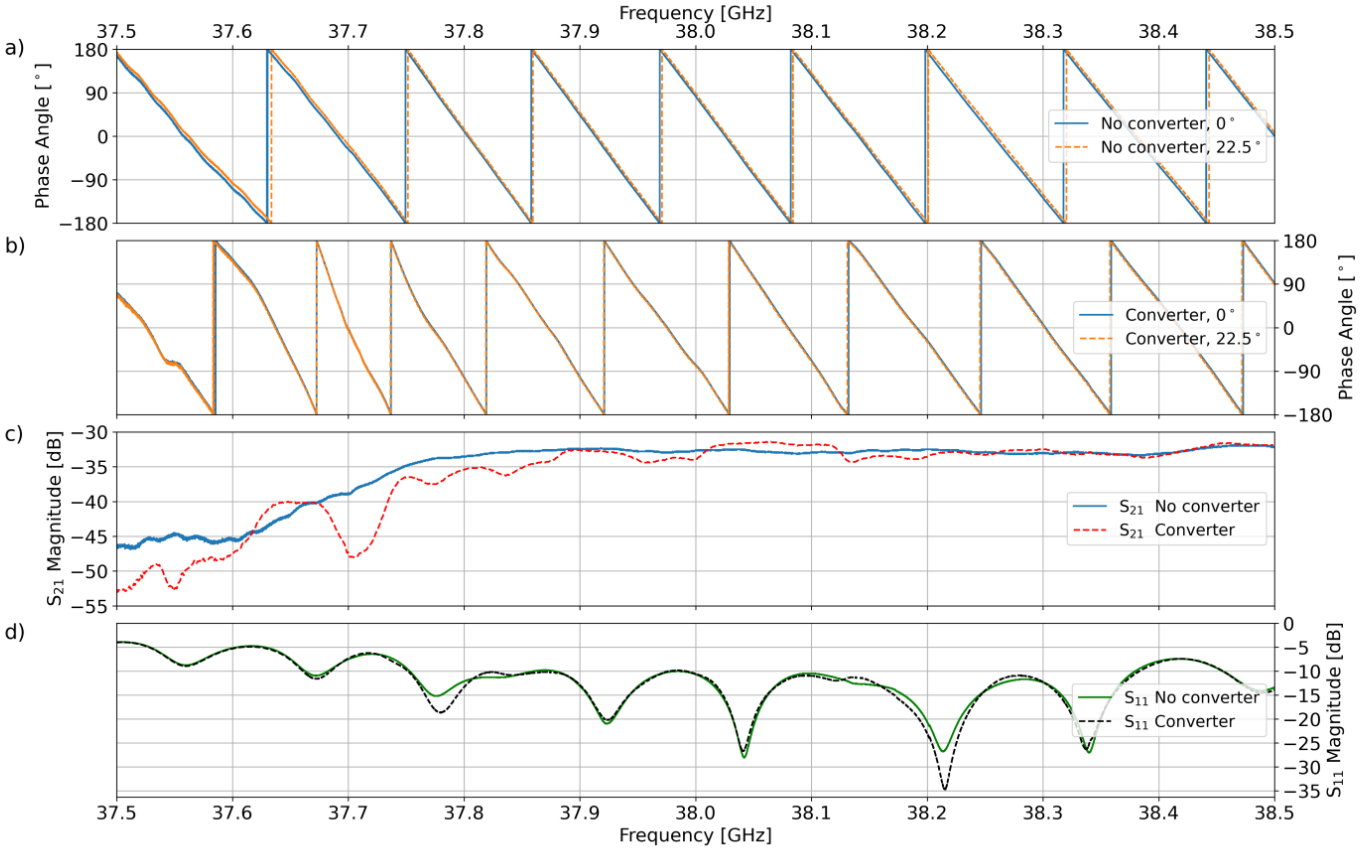

Fig. 13. Phase angle evolution of (a) $TE_{2,1}$, (b) $TE_{2,1}$ signal and $TE_{2,2}$ signals, after passing through the coharmonic corrugated waveguide with "orthogonal" polarizations and (c) transmission and (d) reflection far-field *S*-parameter measurements for the coharmonic corrugated waveguide both with and without the ripple wall mode converter. In (a) and (b), the two profiles overlap each other.

without it, thus subjecting the cavity to both the $TE_{2,1}$ and $TE_{2,2}$ modes over the spectral range of 37.6–37.8 GHz.

The resulting phase behavior for both cavity orientations is seen in Fig. 13, for situation where the ripple wall mode converter is not present [Fig. 13(a)] and when the ripple wall converter is present [Fig. 13(b)].

For the case of purely $TE_{2,1}$ signal [Fig. 13(a)], the phase evolution is smooth across the entire frequency band, showing no significant change in gradient. When the ripple wall mode convertor is installed [Fig. 13(b)], the gradient of the phase evolution clearly varies across the frequency range. In the region of 37.65–37.75 GHz, the phase evolution is much more rapid, implying the excitation of the $TE_{2,2}$ mode which will be closer to cutoff (and therefore exhibit a more rapid phase evolution with frequency) in the ripple wall mode convertor, the azimuthally corrugated waveguide, and (weakly) the output taper. On examining the transmission *S*-parameters of the ripple wall mode converters (Fig. 11), this frequency range clearly corresponds to where the transmitted signal displays a significant drop in magnitude, corresponding to the excitation of the $TE_{2,2}$ mode.

That the cavity is being tested in the $TE_{2,2}$ mode around 37.7 GHz is further verified if we consider the amplitude component of the *S*-parameters measured in the far-field of the launching antenna with and without the ripple wall mode converter, as shown in Fig. 13(c). Here, a clear dip in the S_{21} parameter is evident around 37.7 GHz only when the ripple wall converter is installed (the detector was located in a near-optimum location to measure the radiation launched from the antenna in the $TE_{2,1}$ mode). In contrast, the profile observed without the ripple wall converter shows a progressive drop in signal as the $TE_{2,1}$ launcher approaches its minimum frequency. On considering the corresponding S_{11} parameters [Fig. 13(d)], around 37.7 GHz, no major change is introduced by the rippled wall converter—implying that the energy has been radiated, but into a different (much wider) radiation pattern.

As a result, we can say with confidence that the $TE_{2,2}$ mode is excited at 37.7 GHz, ~100 MHz lower than its design frequency. Fig. 13(c) shows that the bandwidth of the coupling is ~50 MHz. Due to the tolerance of the CNC lathe in the machining of the aluminum former, we suspect the amplitude and period of the ripple within the ripple wall mode converter are not consistent along its length. As seen in Fig. 11, multiple instances of weak mode conversion are observed across the frequency span, indicating the imperfection in the construction of the mode converter. This behavior is within the sensitivity of the manufacturing tolerances discussed previously in Section III-A.

Critically in Fig. 13(a) and (b), irrespective of the angular orientation of the azimuthally corrugated waveguide, the phase evolution of the signal is completely unaffected, both in regions and conditions where the signal is in the $TE_{2,1}$ and $TE_{2,2}$ modes. This verifies that the dispersion of the

Authorized licensed use limited to: University of York. Downloaded on August 29,2024 at 10:33:34 UTC from IEEE Xplore. Restrictions apply.

quadrupole modes is insensitive to their relative polarization with respect to the structure of an eightfold azimuthal corrugation in a waveguide.

V. Conclusion

The insensitivity of the dispersion of a coharmonic corrugated waveguide to the polarization of quadrupole ($TE_{2,n}$) modes has been analyzed both numerically and experimentally. The sensitivity of the performance of ripple wall mode converters to the amplitude of their corrugation has also been calculated. The tight tolerances can reasonably account for minor discrepancies observed between the S-parameters predicted by CST Microwave Studio and those measured experimentally. Although designed to operate at a frequency of 37.82 GHz, analysis of data demonstrated that the ripple wall mode converter converts into the $TE_{2,2}$ mode at a frequency of 37.7 GHz. However, since this is above the cutoff frequency of the coharmonic corrugated waveguide and the $TE_{2,1}$ launching system, the insensitivity of the dispersion to the mode polarization has been demonstrated successfully.

Acknowledgment

The authors wish to thank D. Barclay for his assistance in preparing the components described in this article, as well as A. V. Savilov, I. V. Bandurkin, and V. L. Bratman from the Institute of Applied Physics, Russian Academy of Sciences, Nizhny Novgorod, for discussions on the coharmonic gyro-multiplier.

References

[1] J. L. Hirshfield, "Coherent radiation from spatiotemporally modulated gyrating electron-beams," *Phys. Rev. A, Gen. Phys.*, vol. 44, pp. 6845–6853, Nov. 1991.

[2] G. S. Nusinovich and O. Dumbrajs, "Two-harmonic prebunching of electrons in multicavity gyrodevices," *Phys. Plasmas*, vol. 2, no. 2, pp. 568–577, Feb. 1995.

[3] Q. S. Wang, D. B. McDermott, and N. C. Luhmann, "Demonstration of marginal stability theory by a 200-kW second-harmonic gyro-TWT amplifier," *Phys. Rev. Lett.*, vol. 75, no. 23, pp. 4322–4325, Dec. 1995.

[4] G. S. Nusinovich, B. Levush, and O. Dumbrajs, "Optimization of multistage harmonic gyrodevices," *Phys. Plasmas*, vol. 3, no. 8, pp. 3133–3144, Aug. 1996.

[5] B. G. Danly, B. Levush, V. L. Granatstein, W. G. Lawson, G. S. Nusinovich, and M. T. Walter, "Design of a frequency-doubling, 35-GHz, 1-MW gyroklystron," *IEEE Trans. Plasma Sci.*, vol. 28, no. 3, pp. 688–694, Jun. 2000.

[6] D. Dragoman and M. Dragoman, "Terahertz fields and applications," *Prog. Quantum Electron.*, vol. 28, no. 1, pp. 1–66, Jan. 2004.

[7] P. H. Siegel, "Terahertz technology," *IEEE Trans. Microw. Theory Techn.*, vol. 50, no. 3, pp. 910–928, Mar. 2002.

[8] T. Nagatsuma *et al.*, "Terahertz wireless communications based on photonics technologies," *Opt. Exp.*, vol. 21, nos. 20, pp. 23736–23747, Sep. 2013.

[9] P. H. Siegel, "THz instruments for space," *IEEE Trans. Antennas Propag.*, vol. 55, no. 11, pp. 2957–2965, Nov. 2007.

[10] P. U. Jepsen, D. G. Cooke, and M. Koch, "Terahertz spectroscopy and imaging—Modern techniques and applications," *Laser Photon. Rev.*, vol. 5, no. 1, pp. 124–166, Jan. 2011.

[11] P. H. Siegel, "Terahertz technology in biology and medicine," *IEEE Trans. Microw. Theory Techn.*, vol. 52, no. 10, pp. 2438–2447, Oct. 2004.

[12] E. Pickwell and V. P. Wallace, "Biomedical applications of terahertz technology," *J. Phys. D, Appl. Phys.*, vol. 39, pp. R301–R310, Sep. 2006.

[13] T. Idehara and S. P. Sabchevski, "Development and applications of high-frequency gyrotrons in FIR FU covering the sub-THz to THz range," *J. Infr. Millim. THz Waves*, vol. 33, no. 7, pp. 667–694, Jan. 2012.

[14] E. A. Nanni, A. B. Barnes, R. G. Griffin, and R. J. Temkin, "THz dynamic nuclear polarization NMR," *IEEE Trans. THz Sci. Technol.*, vol. 1, no. 1, pp. 145–163, Sep. 2011.

[15] V. A. Flyagin, A. V. Gaponov, M. I. Petelin, and V. K. Yulpatov, "The gyrotron," *IEEE Trans. Microw. Theory Techn.*, vol. MTT-25, no. 6, pp. 514–521, Jun. 1977.

[16] V. A. Flyagin and G. S. Nusinovich, "Gyrotron oscillators," *Proc. IEEE*, vol. 76, no. 6, pp. 644–656, Jun. 1988.

[17] A. A. Andronov, "The gyrotron—High-power source of millimeter and submillimeter waves," *Infr. Phys.*, vol. 18, pp. 385–393, Dec. 1978.

[18] I. V. Bandurkin, V. L. Bratman, and A. V. Savilov, "Frequency multiplication in gyrotron autooscillators," *Tech. Phys. Lett.*, vol. 32, no. 1, pp. 84–87, Jan. 2006.

[19] I. V. Bandurkin, V. L. Bratman, A. V. Savilov, S. V. Samsonov, and A. B. Volkov, "Experimental study of a fourth-harmonic gyromultiplier," *Phys. Plasmas*, vol. 16, no. 7, Jul. 2009, Art. no. 070701.

[20] D. A. Constable *et al.*, "Numerical simulations of a co-harmonic gyrotron," *J. Phys. D, Appl. Phys.*, vol. 45, no. 6, Jan. 2012, Art. no. 065105.

[21] D. A. Constable *et al.*, "A co-harmonic gyro-oscillator with a novel interaction cavity," in *Proc. 10th IEEE Int. Vac. Electron. Conf.*, Rome, Italy, Apr. 2009, pp. 233–234.

[22] I. V. Bandurkin, Y. K. Kalynov, I. V. Osharin, and A. V. Savilov, "Gyrotron with a sectioned cavity based on excitation of a far-from-cutoff operating mode," *Phys. Plasmas*, vol. 23, no. 1, Jan. 2016, Art. no. 013113.

[23] A. V. Savilov, "High-harmonic gyrotron with sectioned cavity," *Appl. Phys. Lett.*, vol. 95, no. 7, Aug. 2009, Art. no. 073503.

[24] I. V. Bandurkin, Y. K. Kalynov, and A. V. Savilov, "Experimental realization of the high-harmonic gyrotron oscillator with a klystron-like sectioned cavity," *IEEE Trans. Electron Devices*, vol. 62, no. 7, pp. 2356–2359, Jul. 2015.

[25] I. V. Bandurkin and S. V. Mishakin, "Gyromultiplier with sectioned cavity," *Phys. Plasmas*, vol. 17, Nov. 2010, Art. no. 110706.

[26] W. Lawson, "The design of a high-power, high-gain, frequency-doubling gyroklystron," *IEEE Trans. Plasma Sci.*, vol. 33, no. 2, pp. 858–865, Apr. 2005.

[27] W. Lawson, R. L. Ives, M. Mizuhara, J. M. Neilson, and M. E. Read, "Design of a 10-MW, 91.4-GHz frequency-doubling gyroklystron for advanced accelerator applications," *IEEE Trans. Plasma Sci.*, vol. 29, no. 3, pp. 545–558, Jun. 2001.

[28] D. A. Constable *et al.*, "Magic 3-D simulations of a 1.37 THz gyro-multiplier," in *Proc. 14th IEEE Int. Vac. Electron. Conf.*, Paris, France, Sep. 2013, Art. no. 6571128.

[29] G. S. Nusinovich, O. V. Sinitsyn, and T. M. Antonsen, "Mode switching in a gyrotron with azimuthally corrugated resonator," *Phys. Rev. Lett.*, vol. 98, no. 20, May 2007, Art. no. 205101.

[30] D. A. Constable, "The numerical and experimental investigation of gyro-multiplier configurations," M.S thesis, SUPA, Dept. Phys., Univ. Strathclyde, Glasgow, U.K., 2013.

[31] D. A. Constable, X. S. Fampris, K. Ronald, W. He, C. G. Whyte, and C. W. Robertson, "A novel cylindrical $TE_{2,1}$ mode converter," *Rev. Sci. Instrum.*, vol. 81, no. 9, Sep. 2010, Art. no. 094702.

[32] W. Lawson, M. Esteban, H. Raghunathan, B. P. Hogan, and K. Bharathan, "Bandwidth studies of TE_{0n}-$TE_{0(n+1)}$ ripple-wall mode converters in circular waveguide," *IEEE Trans. Microw. Theory Techn.*, vol. 53, no. 1, pp. 372–379, Jan. 2005.

[33] R. A. Schill and S. R. Seshadri, "Optimization of a bumpy cylindrical wave-guide mode converter," *J. Infr. Millim. THz Waves*, vol. 7, pp. 1129–1167, Aug. 1986.

[34] M. Thumm, "High-power millimetre-wave mode converters in overmoded circular waveguides using periodic wall perturbations," *Int. J. Electron.*, vol. 57, no. 6, pp. 1225–1246, Dec. 1984.

[35] N. F. Kovalev, I. M. Orlova, and M. I. Petelin, "Wave transformation in a multimode waveguide with corrugated walls," *Radiophys. Quantum Electron.*, vol. 11, pp. 783–786, Nov. 1968.

[36] C. Moeller, "Mode converters used in the doublet III ECH microwave system," *Int. J. Electron.*, vol. 53, no. 6, pp. 587–593, Dec. 1982.

[37] M. Thumm, H. Kumric, and H. Stickel, "TE_{03} to TE_{01} mode converters for use with a 150 GHz gyrotron," *Int. J. Infr. Millim. Waves*, vol. 8, no. 3, pp. 227–240, Mar. 1987.

[38] M. Thumm, "High power mode conversion for linearly polarized HE_{11} hybrid mode output," *Int. J. Electron.*, vol. 61, no. 6, pp. 1135–1153, Dec. 1986.

Authorized licensed use limited to: University of York. Downloaded on August 29,2024 at 10:33:34 UTC from IEEE Xplore. Restrictions apply.